

# Learning Deep Hybrid Models with Sharpness-Aware Minimization

Naoya Takeishi<sup>1</sup>

## Abstract

Hybrid modeling, the combination of machine learning models and scientific mathematical models, enables flexible and robust data-driven prediction with partial interpretability. However, effectively the scientific models may be ignored in prediction due to the flexibility of the machine learning model, making the idea of hybrid modeling pointless. Typically some regularization is applied to hybrid model learning to avoid such a failure case, but the formulation of the regularizer strongly depends on model architectures and domain knowledge. In this paper, we propose to focus on the flatness of loss minima in learning hybrid models, aiming to make the model as simple as possible. We employ the idea of sharpness-aware minimization and adapt it to the hybrid modeling setting. Numerical experiments show that the SAM-based method works well across different choices of models and datasets.

## 1. Introduction

Combining models from two contrasting regimes, scientific mathematical models and machine learning models, can be useful for improving generalization, robustness, and partial interpretability of prediction. The combination of the two has been actively studied in various fields, including weather forecasting (Xu et al., 2024; Verma et al., 2024), robotics (Ajay et al., 2018; Salzmann et al., 2023; Heiden et al., 2021; Gao et al., 2024), and healthcare (Miller et al., 2020; Kashtanova et al., 2022; Palumbo et al., 2025).

Such *hybrid modeling* is, while being conceptually simple and intuitive, sometimes not so straightforward. In particular, when a machine learning model is too flexible compared to a scientific model to be combined with, hybrid modeling may become pointless, with the machine learning part fitting to all the data variation and the scientific model left unused (Yin et al., 2021; Takeishi & Kalousis, 2021; 2023; Zou

<sup>1</sup>School of Engineering, The University of Tokyo, Japan. Correspondence to: Naoya Takeishi <ntake@g.ecc.u-tokyo.ac.jp>.

et al., 2024; Wehenkel et al., 2023). In other words, the unknown parameters of a scientific model, if any, may become unidentifiable regardless of their original identifiability.

A way to mitigate the potential issue in hybrid modeling is to regularize the machine learning part, mostly a deep neural net, so that the scientific model is adequately utilized. For example, suppose an additive hybrid model  $y = f(x) + g(x)$ , where  $f$  and  $g$  are a scientific model and a neural net, respectively, where both have unknown parameters. In learning such additive models, minimizing  $\|g\|$  intuitively sounds a natural regularizer to suppress the excess flexibility of  $g$ , as indeed practiced by, e.g., Yin et al. (2021). Then how should we do about a hybrid architecture like  $y = g(x, f(x))$ ? How about  $y = g_3(x, f_1(x, g_2(x)) \cdot g_1(f_2(x)))$ , and whatever? For general hybrid architectures, designing the regularizer is often challenging with various functional forms and complex function compositions.

In this paper we aim to develop a versatile method applicable to any model architectures to (partially) address the unidentifiability of hybrid models. We hypothesize that *seeking flat minima of the loss can help identify scientific parameters*, at least to some extent. Flatness has often been discussed in connection with generalization and model complexity (e.g., Hochreiter & Schmidhuber, 1997). Our idea is to keep the machine learning part of hybrid models simple to make the maximum use of the scientific model part, by seeking flat minima of the loss. We propose to use a variant of sharpness-aware minimization (SAM) (Foret et al., 2021) for learning deep hybrid models. The proposed method only depends on the flatness of loss functions and thus is applicable regardless of model architectures.

SAM has recently been actively studied in the community, where the main interest has been on the improvement of generalization by SAM and its variants. In this work we do not develop a totally new variant of SAM; our own contribution rather lies in the adaptation of SAM in the hybrid modeling context and the demonstration of its effectiveness in improving the identification of scientific parameters. From the hybrid modeling point of view, the proposed method is unique in the sense that it is applicable to general hybrid architectures without relying on specific model forms or additional calibration data.

## 2. Preliminaries

### 2.1. Hybrid Modeling

Suppose a prediction task to predict  $y \in \mathcal{Y}$  from  $x \in \mathcal{X}$ . This restriction is purely for the sake of notational simplicity, and the discussion below can be easily extended to more general settings. Let

$$f_\theta : \mathcal{X} \rightarrow \mathcal{Z} \quad \text{and} \quad g_\phi : \mathcal{X} \times \mathcal{Z} \rightarrow \mathcal{Y}$$

be a scientific mathematical model and a machine learning model (e.g., a deep neural net) parametrized by  $\theta$  and  $\phi$ , respectively.  $\mathcal{Z}$  is the space of the output of the scientific model. Importantly, we suppose the scientific model,  $f_\theta$ , is incomplete in some sense, so combining it with the machine learning model makes sense.

Unless stated otherwise, we consider the combination of the two as a general function composition:

$$h_{\theta, \phi}(x) = g_\phi(x, f_\theta(x)). \quad (1)$$

While more complex, nested compositions can be considered as well, we stick to this simple form for clarity. Note also that hybrid models in practice may contain further operations such as numerical integration over time; for example, it is typical to use hybrid neural ODEs,  $y = \text{ODESolve}(h_{\theta, \phi}(x; t) = 0)$ , in modeling dynamical systems. We omit such operations too for simplicity.

We informally assume the following three: First,  $g_\phi$  is sufficiently flexible to approximate arbitrary functions from (compact subsets of)  $\mathcal{X} \times \mathcal{Z}$  to  $\mathcal{Y}$ ; this is usually the case when  $g_\phi$  is a deep neural net. Second, we have data of  $x \in \mathcal{X}$  and  $y \in \mathcal{Y}$  only, and  $z = f_\theta(x) \in \mathcal{Z}$  is not observable; if it were, doing hybrid modeling would become meaningless. Third,  $f_\theta$ 's parameters would be identifiable if we had sufficient data of  $x$  and  $z$ ; i.e., the scientific model,  $f_\theta$ , originally possesses structural and practical identifiability (see, e.g., [Guillaume et al., 2019](#); [Anstett-Collin et al., 2020](#); [Wieland et al., 2021](#)).

Due to the flexibility of  $g_\phi$  and the unobservability of  $z$ , we face a risk that the hybrid model,  $h_{\theta, \phi}$ , can fit to all the data variation by adjusting only the neural net's parameters,  $\phi$ , regardless of the scientific model's parameters,  $\theta$ . Let  $L_S(\theta, \phi)$  be a loss on a training dataset  $S$ ; for example,

$$L_S(\theta, \phi) = \sum_{(x, y) \in S} \|y - h_{\theta, \phi}(x)\|^2.$$

The empirical risk minimization,

$$\begin{aligned} \min_{\theta, \phi} L_S(\theta, \phi) &= \min_{\theta} L_S(\theta, \phi^*(\theta)) \\ \text{where } \phi^*(\theta) &:= \arg \min_{\phi} L_S(\theta, \phi), \end{aligned}$$

does not have a power to identify  $\theta$  when the profile loss uniformly reaches a small level  $\varepsilon$ , i.e.,

$$L_S(\theta, \phi^*(\theta)) \approx \varepsilon$$

for all  $\theta$ , and thus it does not have clear minima (or has too many insignificant minima). Such a situation, or something close, can happen when  $g_\phi$  is a flexible model, such as deep neural nets. Consequently, the scientific model,  $f_\theta$ , becomes unused, and the merits of hybrid modeling become lost ([Yin et al., 2021](#); [Takeishi & Kalousis, 2021; 2023](#)).

A natural circumvention to break the tie in the profile loss is to incorporate a constraint or regularizer. Such a regularizer should suppress the excess flexibility of the machine learning part and encourage the use of the scientific model in prediction. For instance, consider an additive hybrid model

$$h_{\theta, \phi}(x) = f_\theta(x) + g_\phi(x).$$

[Yin et al. \(2021\)](#) suggested suppressing the flexibility of  $g_\phi$  by penalizing its functional norm,  $\|g_\phi\|$ . Valid formulation of the regularizers heavily depends on task definition and model architectures; unlike the additive form that allows an intuitive design of the regularizer, it is unclear how we should proceed with more complex hybrid architectures.

### 2.2. Flatness, Generalization, and Model Simplicity

Flatness of the minima of a loss function has been discussed in connection with the generalization of machine learning models (e.g., [Hinton & van Camp, 1993](#); [Hochreiter & Schmidhuber, 1997](#); [Baldassi et al., 2016](#); [Dziugaite & Roy, 2017](#); [Chaudhari et al., 2017](#); [Keskar et al., 2017](#); [Izmailov et al., 2018](#)). Flat minima are intuitively understood as wide valleys in the loss landscape, where the loss remains low even if the parameters are perturbed within a certain range. Researchers have studied the advantage of flat minima in generalization, both theoretically and empirically, often with concrete evidence of performance improvement in well-known tasks such as image classification.

One of the rationales of flat minima for better generalization is the correspondence between flatness and model simplicity. For example, [Hochreiter & Schmidhuber \(1997\)](#) connected flat minima with model complexity in terms of minimum description length ([Rissanen, 1978](#)). At a flat minimum, relatively low precision is needed to describe the model's parameters maintaining the performance, thus the model is simple in the sense that the description length is short. [Hochreiter & Schmidhuber \(1997\)](#) also argued that mere flatness is not sufficient to ensure a short description length and that a minimum should be equally flat for each parameter. It is also notable that, as discussed by [Dinh et al. \(2017\)](#), the flatness of a loss function may be arbitrarily scaled without altering a function's outcomes. Such discussions imply the importance of careful definition of flatness (see, e.g., [Tsuzuku et al., 2020](#)).

### 2.3. Sharpness-Aware Minimization

SAM (Foret et al., 2021) is a method to learn deep neural nets with the flatness (or sharpness) of the loss landscape taken into account. SAM and its variants (e.g., Kwon et al., 2021; Kim et al., 2022; Zhuang et al., 2022) have been shown to improve the generalization capability of deep neural nets in typical tasks such as image classification.

The idea of SAM is to minimize the worst-case loss within a certain neighborhood around the current parameters. Let  $L_S(w)$  be a loss function on a training dataset  $S$  for parameters  $w$  of a model. SAM tries to solve the following minimax problem:

$$\min_w \max_{\|\epsilon\| \leq \rho} L_S(w + \epsilon),$$

where  $\rho > 0$  is a hyperparameter that defines the size of the neighborhood. The inner maximization can be approximated by a single step of gradient ascent, yielding the perturbation:

$$\epsilon_{\text{SAM}}^* = \rho \frac{\nabla L_S(w)}{\|\nabla L_S(w)\|}. \quad (2)$$

The update rule of SAM is then given as

$$w \leftarrow w - \eta \nabla L_S(w + \epsilon_{\text{SAM}}^*),$$

where  $\eta > 0$  is the learning rate. The update step is performed by 1) computing the perturbation at the current parameter, 2) evaluating the loss gradient at the perturbed point, and 3) updating the parameter with the computed gradient. In practice the higher-order derivative through  $\epsilon^*$  is usually ignored (Foret et al., 2021).

To compute and minimize the sharpness in a meaningful manner, the geometry of the parameter manifold should be taken into account. It has been addressed by multiple researchers based on different ideas. For example, Kwon et al. (2021) proposed adaptive SAM to scale the perturbation by the magnitude of each parameter, i.e.,

$$\epsilon_{\text{ASAM}}^* = \rho \frac{w^2 \nabla L_S(w)}{\|w \nabla L_S(w)\|} \quad (\text{elementwise}). \quad (3)$$

Kim et al. (2022) proposed to use the loss curvature information for scaling. Let  $F(w)$  be the expected Hessian matrix of the loss (i.e., the Fisher information matrix) at  $w$ . Then, FisherSAM defines the perturbation as

$$\epsilon_{\text{FSAM}}^* = \rho \frac{F(w)^{-1} \nabla L_S(w)}{\sqrt{\nabla L_S(w)^\top F(w)^{-1} \nabla L_S(w)}}, \quad (4)$$

meaning that the perturbation is scaled by the local curvature of the loss landscape.

### 3. Flatness in Hybrid Modeling

#### 3.1. Why Flatness May Help Hybrid Models

We study based on the following idea: in a hybrid model, the machine learning part should be kept simple in order to make the maximum use of the scientific model part. It follows the Occam's razor principle that simpler models are preferred when multiple models explain the data equally well. As any values of the scientific parameters  $\theta$  can yield a small training loss due to the flexibility of the machine learning part  $g_\phi$ , we should choose  $\theta$  so that the corresponding machine learning part  $g_{\phi^*(\theta)}$  (and thus the overall hybrid model) becomes as simple, in some sense, as possible.

Let us discuss the simplicity (or complexity) of a fitted function in terms of the number of bits required, under some prior distribution, to describe the posterior distribution of the parameters. It is given by the KL divergence:

$$\text{KL}(q \parallel p),$$

where  $p$  and  $q$  are prior and posterior distributions of the parameters, respectively (Hinton & van Camp, 1993). For a hybrid model in Equation (1) with the parameters  $(\theta, \phi)$ , consider a factorized prior distribution  $p(\theta, \phi) = p(\theta)p(\phi)$  and a general posterior distribution  $q(\theta, \phi)$ . The KL divergence then can be decomposed as

$$\begin{aligned} \text{KL}(q(\theta, \phi) \parallel p(\theta, \phi)) &= \underbrace{\text{KL}(q(\theta) \parallel p(\theta)) + \text{KL}(q(\phi) \parallel p(\phi))}_{\text{marginal KL divergence from prior}} \\ &\quad + \underbrace{\text{KL}(q(\theta, \phi) \parallel q(\theta)q(\phi))}_{\text{mutual info under posterior}}, \end{aligned} \quad (5)$$

where  $q(\theta)$  and  $q(\phi)$  are the marginals of  $q(\theta, \phi)$ .

Let us (informally) analyze the behavior of the KL divergence in Equation (5) in accordance with how the hybrid model is learned. First, assume that the learning process is reasonably regularized by the prior, and thus the marginal KLS, i.e., the first two terms of the right-hand side of Equation (5), are similarly small and are not primarily influential in determining the overall KL. Moreover, suppose that the prior is set fairly noninformative as depicted in Figure 1a, which further motivates us to focus on the remaining term.

The last term of Equation (5) is the mutual information between  $\theta$  and  $\phi$  under the posterior,  $q$ . When the probability mass of  $q(\theta)$  spreads over a wide range of  $\theta$  values (i.e.,  $\theta$  is not well identified), the posterior of  $\phi$  would have its probability mass over different  $\phi$  values *adaptively to*  $\theta$ , as shown in Figure 1b, because the machine learning part would be learned so that it works adaptively to  $\theta$  for achieving small loss for any  $\theta$ . Consequently,  $\phi$  would become highly dependent on  $\theta$  under  $q$ , and thus the mutual information would become large. Contrastingly, when  $q(\theta)$  is

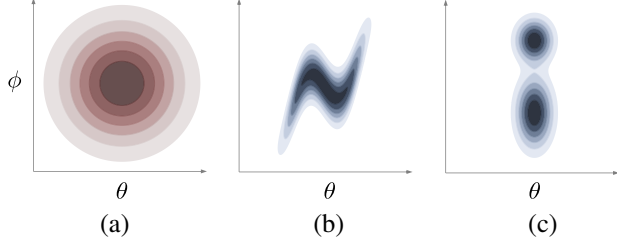


Figure 1. Illustrations of (a) a prior distribution  $p(\theta, \phi)$ ; (b) a posterior distribution  $q(\theta, \phi)$  with nonnegligible mutual information between  $\theta$  and  $\phi$  (i.e., the last term of Equation (5)); and (c) a posterior distribution with small mutual information.  $\theta$  and  $\phi$  are much higher dimensional in reality.

concentrated around a certain  $\theta$  value (i.e.,  $\theta$  is well identified), the dependence between  $\theta$  and  $\phi$  would be milder as illustrated in Figure 1c, and thus the mutual information would relatively be small.

One may think we then should directly minimize the mutual information term in Equation (5) to get a good hybrid model. However, dealing with the dependency between  $\theta$  and  $\phi$  in the posterior is usually intractable. Most working methods for Bayesian neural network inference use posterior approximations that assume independence between parameters. Under such independent posteriors the mutual information is always approximated as zero, and thus minimizing it does not make sense. Even if the independence assumption is not placed, efficiently computing mutual information from a small number of samples is challenging.

Let's get back to the fact that the KL divergence in Equation (5),

$$\text{KL}(q(\theta, \phi) \parallel p(\theta, \phi)),$$

specifies the number of bits to describe the hybrid model. We adopt the idea of seeking flat minima (e.g., Hinton & van Camp, 1993; Hochreiter & Schmidhuber, 1997; Chaudhari et al., 2017; Dziugaite & Roy, 2017) to achieve a simple model, because, as we have reviewed earlier, flat minima are expected to achieve smaller precision to describe the model. To this end we use SAM (Foret et al., 2021) with slight modification as explained in Section 3.2.

Note that the discussion above only informally implies a connection between the identification of  $\theta$ , the model simplicity, and the loss flatness, based on the hypothetical principle that the machine learning part of a hybrid model should be kept simple to identify  $\theta$ . We have not provided (or maybe cannot do so) a sufficient condition for the identification, since we did not assume anything particular about data or model architectures for generality. Rather, the generality is the key here; we aim to propose a method to learn hybrid models without strong assumptions on data and model. Our claim is about the possible utility of seeking flatness in hybrid modeling, which is examined empirically in Section 5.

### Algorithm 1 SAM for hybrid models

**Require:** Number of epochs  $M$ , training dataset  $S$ , loss  $\ell(\cdot, \cdot)$ , learning rates  $\eta_\theta, \eta_\phi$ , perturbation radius  $\rho_\phi$

**Ensure:** Learned parameters  $\theta, \phi$

```

1: Initialize parameters  $\theta, \phi$ 
2: for epoch = 1 to  $M$  do
3:   for each minibatch  $B \subset S$  do
4:      $L_B(\theta, \phi) \leftarrow \frac{1}{|B|} \sum_{(x,y) \in B} \ell(h_{\theta, \phi}(x), y)$ 
5:      $\epsilon_\phi^* \leftarrow$  Eq. (2), (3), or (4) (or others) with  $w = \phi$ 
6:      $\tilde{d}_\theta \leftarrow \nabla_\theta L_B(\theta, \phi + \epsilon_\phi^*)$ 
7:      $\tilde{d}_\phi \leftarrow \nabla_\phi L_B(\theta, \phi + \epsilon_\phi^*)$ 
8:      $\theta \leftarrow \theta - \eta \tilde{d}_\theta, \quad \phi \leftarrow \phi - \eta \tilde{d}_\phi$ 
9:   end for
10: end for

```

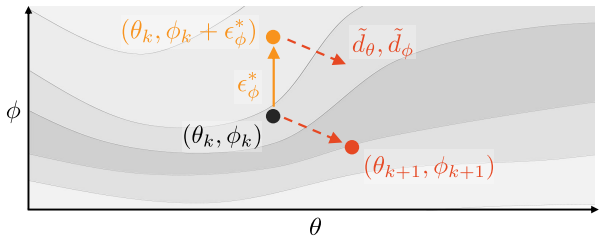


Figure 2. Update step of Algorithm 1, at the  $k$ -th iteration.

### 3.2. SAM for Hybrid Models

We suggest using SAM (Foret et al., 2021) to seek flat (or non-sharp) minima of the loss function in learning hybrid models. The overall learning method is shown in Algorithm 1. Similarly to ordinary SAM methods, at each step we first compute the direction  $\epsilon_\phi^*$  to ascend the loss surface, for which the techniques of SAM variants, such as adaptive SAM (Kwon et al., 2021) and Fisher SAM (Kim et al., 2022), can also be used. We then compute the gradient at the perturbed point, go back to the original point storing the gradient, and finally do the update with the gradient.

Algorithm 1 is slightly modified from ordinary SAMs in that the parameter perturbation is computed only in the  $\phi$  direction, as depicted in Figure 2. Because it is the machine learning part  $g_\phi$  that should be simple for the maximum use of the scientific part, SAM should reach a value of  $\phi$  around which the loss is flat. On the other hand, nothing requires the flatness along the direction of  $\theta$ . On the contrary, the loss basically should *not* be flat along  $\theta$ ; being flat along  $\theta$  means different values of  $\theta$  achieve similarly small loss values, implying  $\theta$  is hard to identify. The inherent identifiability of  $\theta$  depends on the structural and practical identifiability for the scientific model  $f_\theta$  and should not be harmed. In practice, however, the effect of the modification is not necessarily dominant in performance because a scientific model usually has a small number of parameters.

## 4. Related Work

Hybrid models (or grey-box models, residual physics, etc.) combining scientific mathematical models (also called mechanistic models, physics models, or expert models) and neural nets have been studied for decades (see, e.g., Psichogios & Ungar, 1992; Rico-Martínez et al., 1994; Thompson & Kramer, 1994; Forssell & Lindskog, 1997; Schweidtmann et al., 2024). More recently researchers have been interested in using deep neural nets also in hybrid modeling (e.g. Yin et al., 2021; Takeishi & Kalousis, 2021; 2023; Qian et al., 2021; Haußmann et al., 2021; Mehta et al., 2021; Wehenkel et al., 2023; Tushar & Chakraborty, 2023; Rudolph et al., 2024; Holt et al., 2024; Ye et al., 2024; Giampiccolo et al., 2024; Cohrs et al., 2024; Claes et al., 2025; Thoreau et al., 2025). The application of deep hybrid modeling has been active in various fields such as, to name a few, traffic prediction (Shirakami et al., 2023), weather forecasting (Xu et al., 2024; Verma et al., 2024), robotics (Ajay et al., 2018; Salzmann et al., 2023; Heiden et al., 2021; Gao et al., 2024), disease prediction (Arik et al., 2020), and healthcare (Miller et al., 2020; Kashtanova et al., 2022; Palumbo et al., 2025).

Several researchers have been working on methods to learn deep hybrid models appropriately to ensure the maximum use of scientific mathematical models. Yin et al. (2021) discuss hybrid neural ODEs and propose a method to learn the model by minimizing the functional norm of the neural network part. It is a natural formulation for the additive combination of the scientific model and the neural net, but is not straightforwardly applicable to other forms of hybrid models. Takeishi & Kalousis (2021) propose a regularizer that minimizes the discrepancy between the full hybrid model and a scientific-model-only reduction and apply it to variational autoencoders whose decoder has a hybrid structure. It is in principle applicable to general architectures as long as the reduced model can be defined, but requires a specific design for each architecture. We will examine the performance of these methods in the experiments in Section 5.

Some methods utilize more specific model architectures and additional information. Zou et al. (2024) present a method to use domain knowledge of the effects of interventions to maintain meaningful causal implications. Claes et al. (2025) propose a principled method to properly learn hybrid models when the two parts work on distinct feature sets. Cohrs et al. (2024) suggest using the method of double machine learning for specific types of hybrid models. In the context of simulation-based inference with misspecified simulator, which is very close to the idea of hybrid modeling, Wehenkel et al. (2025) and Senouf et al. (2025) utilize a small amount of calibration data, i.e., data of the output of the scientific model. These methods would work certainly well when the assumptions are met, but in this paper we do not assume such specific architectures or additional data.

## 5. Experiment

### 5.1. Scope

The aim of the experiments is to examine the effectiveness of the proposed method on hybrid modeling tasks. Importantly, we are interested in *how the method helps the identification of scientific parameters in hybrid models*, including architectures for which regularization with the existing methods (Yin et al., 2021; Takeishi & Kalousis, 2021) is not straightforward. Among the tasks introduced in Section 5.2, the first two tasks are already studied in the literature (e.g. Yin et al., 2021) and the existing regularization methods are directly applicable. On the other hand, applying the existing methods to the other four tasks is not straightforward or requires careful design of the regularizers.

Obviously, the performance of the estimation of  $\theta$  can be measured only when some true or reference values of  $\theta$  are available, for which we prepared the synthetic data or referred to the domain knowledge. In this sense any experiments with quantitative evaluation of the estimation remain artificial in principle. With that being said, the point of the empirical evaluation here is to see if the SAM-based method, which does not assume specific model architectures, can work comparably with the learning methods whose exact formulation depends on architectures.

Several methods of hybrid model learning are out of the scope of the current experiments or are not applicable to our tasks. The hybrid models to be tested in the experiments have unknown parameters in both of the scientific and machine learning parts; thus the learning methods used in some hybrid modeling studies (e.g., Haußmann et al., 2021), where the scientific model parameters are fixed, are not of our main interest here. We do not assume at all the access to calibration data, i.e., data of the output of the scientific model,  $z = f_\theta(x)$ ; thus the methods based on partial access to calibration data (Wehenkel et al., 2025; Senouf et al., 2025) are out of the scope. Moreover, none of the methods assuming specific hybrid model architectures or additional information (Zou et al., 2024; Cohrs et al., 2024; Claes et al., 2025) are applicable to our tasks.

### 5.2. Data and Models

We employ six tasks with four synthetic datasets and two real-world datasets. The full details of the tasks can be found in the appendix and the references therein.

**PENDULUM TIME-SERIES** As already practiced in previous studies (e.g., Yin et al., 2021; Takeishi & Kalousis, 2021; Wehenkel et al., 2023), we generated data from the damped pendulum system:

$$\ddot{v}(t) + \gamma \dot{v}(t) + (2\pi\omega)^2 \sin v(t) = 0,$$

where  $v(t)$  is the pendulum's angle, and  $\ddot{v}$  and  $\dot{v}$  are the second and first derivatives with regard to  $t$ , respectively. After generating data, we assume no access to the data-generating values of  $\gamma$  and  $\omega$ . We formulate the task as a sequence prediction from  $x$  to  $y$ :

$$x = \mathbf{v}(0) \in \mathbb{R}^2 \quad \text{and} \\ y = [\mathbf{v}(\Delta t), \dots, \mathbf{v}(m_y \Delta t)] \in \mathbb{R}^{m_y \times 2},$$

where  $\mathbf{v} = [v, \dot{v}]$ ,  $\Delta t$  is the time step, and  $m_y$  is the output sequence length.

In building a hybrid model, we suppose that we only know a part of the equation as an incomplete scientific model:

$$f_\theta(v) := \ddot{v}(t) + (2\pi\tilde{\omega})^2 \sin v(t),$$

where  $\theta = \{\tilde{\omega}\}$  is the unknown parameter to be identified. Then a hybrid neural ODE is formulated as

$$y = \text{ODESolve}(f_\theta(v) + g_\phi(v) = 0; v(0) = x), \quad (6)$$

where  $g_\phi$  is a feed-forward neural net with two hidden layers and the ReLU activation function.

**REACTION-DIFFUSION** We generated data from a reaction-diffusion system:

$$u_t(t, \xi) = a\nabla^2 u + u - u^3 - \kappa - v, \\ v_t(t, \xi) = b\nabla^2 v + u - v,$$

where  $u(t, \xi)$  and  $v(t, \xi)$  are the concentrations of two chemical species at time  $t$  and spatial location  $\xi \in [-1, 1]^2$ ,  $u_t$  and  $v_t$  are the temporal derivatives of  $u$  and  $v$ , respectively, and  $\nabla^2$  is the Laplacian operator with regard to the space. The task is again to predict a sequence of the states  $y \in \mathbb{R}^{m_y \times 2 \times d \times d}$  given an initial condition  $x \in \mathbb{R}^{2 \times d \times d}$ , where  $d = 32$  is the number of spatial discretization points along each axis. We build a hybrid neural PDE model with an incomplete scientific model as the diffusion terms:

$$f_\theta(u, v) := \begin{bmatrix} u_t - \tilde{a}\nabla^2 u \\ v_t - \tilde{b}\nabla^2 v \end{bmatrix},$$

where  $\theta = \{\tilde{a}, \tilde{b}\}$  is the unknown parameters to be identified. The machine learning part  $g_\phi$  is a convolutional neural net.

**DUFFING OSCILLATOR** We generated data from a nonlinear oscillator system:

$$\ddot{v}(t) + \gamma\dot{v}(t) + \alpha v(t) - \beta v(t)^3 = 0.$$

We formulate the task similarly to the preceding tasks, i.e., the prediction from an initial condition  $x \in \mathbb{R}^2$  to a subsequent states  $y \in \mathbb{R}^{m_y \times 2}$ . The hybrid model to be used is again a hybrid neural ODE like Equation (6) with an incomplete scientific model:

$$f_\theta(v) := \ddot{v}(t) + \tilde{\alpha}v(t),$$

where  $\theta = \{\tilde{\alpha}\}$  is the unknown parameter to be identified.

**PENDULUM IMAGES** We first generated trajectories of a pendulum as in the PENDULUM TIME-SERIES task and then created gray-scale images of size  $d \times d$  with  $d = 48$  pixels based on the simulated pendulum angles. The task is to predict future image sequences  $y \in [0, 1]^{m_y \times d \times d}$  given an initial image  $x \in [0, 1]^{d \times d}$ . The hybrid model is built by combining the hybrid neural ODE in Equation (6) and convolutional neural nets for decoding and encoding. The decoder maps the pendulum angle to an image, and the encoder maps the input image to a latent representation including the initial condition of the pendulum. The initial condition is inherently unidentifiable; we are only interested in estimating the pendulum's frequency, i.e.,  $\theta = \{\omega\}$ .

**WIND TUNNEL** We used a dataset comprising measurements from a real-world wind tunnel (Gamella et al., 2025). We extracted a subset of the data to formulate a task to predict  $y \in \mathbb{R}^{m_y}$ , the pressure inside the tunnel, from  $x \in \mathbb{R}^{3m_x}$ , the loads of the intake and exhaust fans and the position of the hatch. The hatch controls an additional opening in the middle of the tunnel. As a scientific model, we use the models “A1” and “C2” presented in Gamella et al. (2025), which give the relation between the pressure and the fan loads. They are incomplete in terms of the effect of the hatch position and the transient dynamics. The hybrid model transforms the output of these models with a feed-forward neural net. We set a scalar parameter of the model C2 as the unknown parameter to be estimated,  $\theta \in \mathbb{R}$ . As the data-generating value of  $\theta$  is never known, we used a value suggested in the paper and the codes (Gamella et al., 2025) as a reference to compute the estimation error of  $\theta$ .

**LIGHT TUNNEL** We used another dataset of Gamella et al. (2025); it contains real-world measurements from a light tunnel made of light sources, linear polarizers, and a light sensor. We use the data to formulate a task to predict the RGB image taken by the sensor,  $y \in [0, 1]^{3 \times 100 \times 100}$ , from the light source configuration and the polarizer angles,  $x \in \mathbb{R}^5$ . As an incomplete scientific model, we use the model “F3” presented in Gamella et al. (2025), which models the effect of the polarizers in a frequency-dependent way. We treat nine parameters in the model F3 as unknown parameters to be estimated, i.e.,  $\theta \in \mathbb{R}^9$ . Our hybrid model transforms the output of the scientific model with a convolutional neural net.

### 5.3. Learning Methods

**Empirical risk minimization (erm)** As a basic learning method, we consider the empirical risk minimization without any regularization on the machine learning part's parameters  $\phi$ , i.e., to minimize the prediction error

$$L_S(\theta, \phi) = \sum_{(x, y) \in S} \|y - h_{\theta, \phi}(x)\|^2.$$

Table 1. Estimation errors of  $\theta$  and prediction errors of  $y$ . For LIGHT TUNNEL, we report the cosine similarity between the estimated and reference  $\theta$ 's because the scale of  $\theta$  is structurally unidentifiable; otherwise the root mean squared errors are reported. The best and the second best results are **bolded** and underlined, respectively. Mean and SD over 5 runs with different random seeds are reported.

		erm	l2reg	freq	sam	asam	fsam
PENDULUM TIME-SERIES	$\theta$ -error ( $\times 10^{-3}$ )	$19.9 \pm 16.86$	<u>2.55</u> $\pm 0.097$	<b>0.37</b> $\pm 0.091$	$4.00 \pm 0.541$	$3.35 \pm 1.080$	$3.74 \pm 0.460$
	$y$ -error ( $\times 10^{-2}$ )	$9.11 \pm 0.131$	$8.00 \pm 0.016$	<u>43.1</u> $\pm 0.421$	$8.21 \pm 0.057$	$8.11 \pm 0.069$	$8.20 \pm 0.055$
REACTION -DIFFUSION	$\theta$ -error ( $\times 10^{-4}$ )	$9.27 \pm 0.694$	<b>0.72</b> $\pm 0.307$	<u>1.26</u> $\pm 0.664$	$2.79 \pm 1.972$	$3.66 \pm 1.669$	$2.80 \pm 1.978$
	$y$ -error ( $\times 10^0$ )	$1.11 \pm 0.001$	$1.11 \pm 0.001$	$1.11 \pm 0.001$	$1.19 \pm 0.005$	$1.25 \pm 0.015$	$1.19 \pm 0.005$
DUFFING OSCILLATOR	$\theta$ -error ( $\times 10^{-2}$ )	$30.8 \pm 2.249$	$13.4 \pm 2.407$	$18.7 \pm 3.668$	<b>1.32</b> $\pm 0.648$	<u>3.22</u> $\pm 1.746$	<b>1.32</b> $\pm 0.905$
	$y$ -error ( $\times 10^{-2}$ )	$6.74 \pm 0.045$	$6.45 \pm 0.011$	$6.75 \pm 0.040$	$6.43 \pm 0.021$	$6.46 \pm 0.022$	$6.43 \pm 0.025$
PENDULUM IMAGES	$\theta$ -error ( $\times 10^{-2}$ )	$12.2 \pm 5.767$	$12.9 \pm 2.789$	$11.7 \pm 5.660$	$5.83 \pm 3.862$	<u>5.48</u> $\pm 3.387$	<b>5.04</b> $\pm 4.251$
	$y$ -error ( $\times 10^{-0}$ )	$9.07 \pm 0.143$	$9.13 \pm 0.270$	$8.98 \pm 0.122$	$9.75 \pm 0.303$	$9.57 \pm 0.146$	$9.59 \pm 0.287$
WIND TUNNEL	$\theta$ -error ( $\times 10^{-2}$ )	$69.6 \pm 0.181$	$69.5 \pm 0.286$	$4.39 \pm 0.088$	<u>2.15</u> $\pm 0.979$	$2.39 \pm 0.773$	<b>1.90</b> $\pm 0.667$
	$y$ -error ( $\times 10^1$ )	$5.31 \pm 0.031$	$5.30 \pm 0.022$	$5.28 \pm 0.029$	$5.11 \pm 0.010$	$5.09 \pm 0.015$	$5.09 \pm 0.010$
LIGHT TUNNEL	$\theta$ cosine sim. $\uparrow$	$0.76 \pm 0.268$	$0.87 \pm 0.228$	<u>0.96</u> $\pm 0.013$	<b>0.98</b> $\pm 0.004$	<b>0.98</b> $\pm 0.008$	<b>0.98</b> $\pm 0.007$
	$y$ -error ( $\times 10^0$ )	$4.16 \pm 0.062$	$4.29 \pm 0.067$	$4.21 \pm 0.047$	$5.03 \pm 0.138$	$8.22 \pm 0.298$	$4.61 \pm 0.022$

**L2 regularization (l2reg)** A straightforward way to regularize the learning is to minimize the L2 norm  $R_p(\phi) = \|\phi\|_2^2$ , i.e., to minimize the regularized risk

$$L_S(\theta, \phi) + \lambda_p R_p(\phi),$$

where  $\lambda_p > 0$  is a tunable hyperparameter.

**Functional regularization (freq)** We employ the idea to suppress the machine learning part's flexibility as a function by penalizing its functional norm (Yin et al., 2021) or the discrepancy between the overall model and the scientific-model-only reduction (Takeishi & Kalousis, 2021).

The exact form of the regularizer depends on model architectures and must be designed accordingly. For the PENDULUM TIME-SERIES, DUFFING OSCILLATOR, and REACTION-DIFFUSION tasks, as  $f_\theta$  and  $g_\phi$  are additively combined, we define the regularizer as the minimization of the function norm (Yin et al., 2021):

$$R_f(\phi) = \frac{1}{|X|} \sum_{x \in X} \|g_\phi(x)\|_2^2,$$

where  $X$  is a set of  $x$  drawn from data or some distribution. For the PENDULUM IMAGES, WIND TUNNEL, and LIGHT TUNNEL tasks, as the models are not additive, we follow the idea of Takeishi & Kalousis (2021); we define the regularizer as the minimization of

$$R_f(\phi) = \frac{1}{|X|} \sum_{x \in X} \|h_{\theta, \phi}(x) - h'_{\theta, \phi'}(x)\|_2^2,$$

where  $h'_{\theta, \phi'}$  is a scientific-model-only reduction of the hybrid model; for instance, for a hybrid model of the form  $h_{\theta, \phi}(x) = g_\phi(x, f_\theta(x))$ , we define  $h'_{\theta, \phi'}(x) = A f_\theta(x)$

with a linear map  $A$ , where  $\phi' = \{A\}$ . Such a linear map is required when the dimensionalities of  $z$  and  $y$  are different; when they are in the same ambient space, we simply fix  $A$  as the identity map. For both definitions, the coefficient  $\lambda_f > 0$  is a hyperparameter.

**SAM family (sam, asam, fsam)** We apply SAM to the learning of hybrid models as motivated in Section 3. Instead of fixing the learning rates as in Algorithm 1, we use adaptive learning rate by Adam. We try three different ways to compute the perturbation direction  $\epsilon_\phi^*$ : the standard SAM (Foret et al., 2021), adaptive SAM (Kwon et al., 2021), and Fisher SAM (Kim et al., 2022). We will refer to these three variants as sam, asam, and fsam, respectively. The tunable hyperparameter is the perturbation radius  $\rho_\phi$ .

## 5.4. Results

**Prediction and estimation errors (Table 1)** The main results are summarized in Table 1, where we show the test prediction error ( $y$ -error) and the estimation error of  $\theta$  ( $\theta$ -error). Overall, the SAM-based methods (sam, asam, and fsam) achieved better or comparable performance to the other methods, despite the fact that they do not assume specific hybrid model architectures. SAM family shows slightly worse  $y$ -errors in some cases, but the degradation is mostly qualitatively insignificant, and if needed we can re-train or finetune  $\phi$  after fixing  $\theta$  to improve the  $y$ -error.

More specifically, for the first two tasks (PENDULUM TIME-SERIES and REACTION-DIFFUSION), the method of Yin et al. (2021), here implemented as freq, should work well because the hybrid models are in the additive form, and these data were already examined by them. The performance of the SAM-based methods is slightly worse than

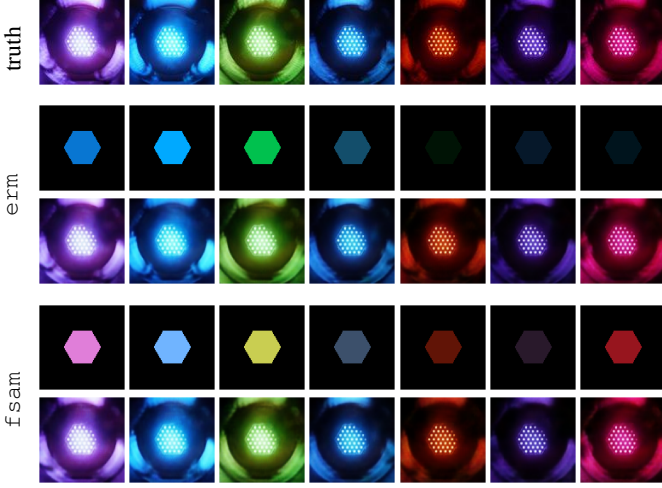


Figure 3. Data and predictions in the LIGHT TUNNEL task: (top row) ground truth images; (middle two rows) predictions from the `erm` model; and (bottom two rows) predictions from the `f.sam` model. For each model, the upper row shows the predictions  $\tilde{z}$  from the scientific model part (model F2), and the lower row shows the full predictions  $\tilde{y}$ .

`12reg` and `freg` but is significantly improved from `erm`. For the remaining tasks (DUFFING OSCILLATOR, PENDULUM IMAGES, WIND TUNNEL, and LIGHT TUNNEL), the baseline methods sometimes did not work well in terms of the estimation of  $\theta$ , which is not surprising because the hybrid models are not in the additive form, and thus these regularization methods need to be specifically designed for each architecture, which is not always straightforward.

**Model behaviors (Figure 3)** Figure 3 shows examples of the predictions in the LIGHT TUNNEL task, where for each method, the upper row is the prediction by the scientific model part,  $\tilde{z} := f_{\tilde{\theta}}(x)$ , whereas the lower row is the full prediction by the hybrid model,  $\tilde{y} = h_{\tilde{\theta}, \tilde{\phi}}(x)$ . The light colors predicted as  $\tilde{z}$  by the `erm` model sometimes obviously deviate from the truth, implying the inadequate use of the scientific model part in the hybrid model due to the misestimation of  $\theta$ . On the other hand, the colors in  $\tilde{z}$  of the `f.sam` model align well with the truth.

**Hyperparameter sensitivity (Figure 4)** We investigate the sensitivity of the performance to the configuration of the hyperparameters:  $\lambda_p$ ,  $\lambda_f$ , and  $\rho_\phi$  for the `12reg`, `freg`, and `{sam, asam, fsam}`, respectively. We show a part of the results in Figure 4; the remaining results are in the appendix. As a reference we also show the performance by the `erm` model with dashed lines. In terms of the  $\theta$ -estimation error, the performance is not very sensitive to the hyperparameter value within the standard range of  $\rho$  (Foret et al., 2021; Kwon et al., 2021; Kim et al., 2022). On the other hand, the  $y$ -prediction error gets significantly worse than the reference by `erm` when the regularization effect becomes too strong.

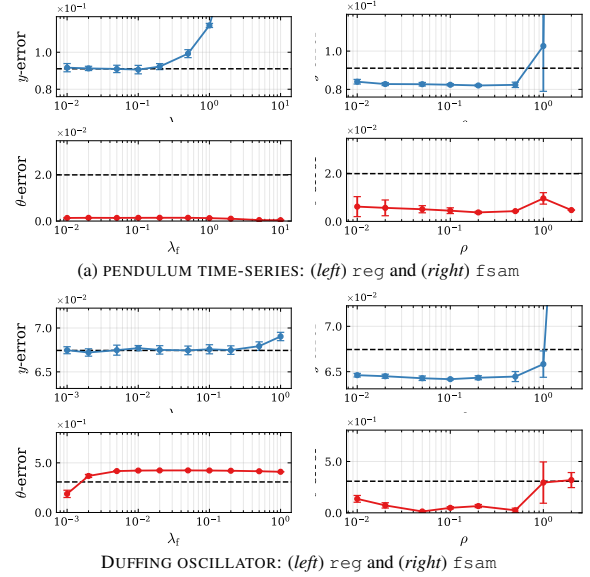


Figure 4. (b) Effects of the hyperparameter configurations. The dashed lines represent the average performance of `erm`.

## 6. Conclusion

In this paper, we suggest using SAM and its variants in hybrid modeling, the combination of scientific mathematical models and machine learning models. The underlying idea is that the machine learning part of a hybrid model should be kept as simple as possible for the maximum use of the scientific model part, and we have hypothesized that SAM is useful to achieve such a simple model. We empirically validated the effectiveness of the idea on different tasks using synthetic and real-world data. An overall observation from the experiments is that SAM is indeed useful for identifying unknown parameters of the scientific model part, despite not requiring specific hybrid model architectures. The SAM-based learning method for hybrid models can be universally applicable to different architectures, unlike the existing regularization methods that require specific design depending on the model architecture.

An important limitation is that unless one has specific assumptions about the data-generating process, the proposed learning method does not necessarily identify *the correct* value of the unknown scientific parameters, as is the case with the existing methods for hybrid modeling. In other words, there is often no such thing like the correct scientific parameter; it solely depends on one's brief about the data-generating process and the principles of model selection. Moreover, our study is currently limited to the intuitive motivation of using SAM and the empirical evidence of its utility in hybrid modeling. More rigorous characterization of the parameter identification in hybrid models is an interesting but challenging open question.

## Acknowledgements

This work was supported by JST PRESTO JPMJPR24T6 and JSPS JP25H01454.

## Impact Statement

This work proposes a method for learning hybrid models that combine scientific mathematical models with machine learning models. While it is difficult to anticipate broader societal consequences at this stage of fundamental research, hybrid modeling is often motivated by the need for more interpretable and reliable machine learning. If deployed in critical settings without sufficient validation, however, hybrid models could still lead to negative outcomes. Therefore, careful evaluation and responsible use are important.

## References

Ajay, A., Wu, J., Fazeli, N., Bauza, M., Kaelbling, L. P., Tenenbaum, J. B., and Rodriguez, A. Augmenting physical simulators with stochastic neural networks: Case study of planar pushing and bouncing. In *Proceedings of the 2018 IEEE/RSJ International Conference on Intelligent Robots and Systems*, pp. 3066–3073, 2018.

Anstett-Collin, F., Denis-Vidal, L., and Millérioux, G. A priori identifiability: An overview on definitions and approaches. *Annual Reviews in Control*, 50:139–149, 2020.

Arik, S. Ö., Li, C.-L., Yoon, J., Sinha, R., Epshteyn, A., Le, L. T., Menon, V., Singh, S., Zhang, L., Yoder, N., Nikoltchev, M., Sonthalia, Y., Nakhost, H., Kanal, E., and Pfister, T. Interpretable sequence learning for COVID-19 forecasting. In *Advances in Neural Information Processing Systems 33*, pp. 18807–18818, 2020.

Baldassi, C., Borgs, C., Chayes, J. T., Ingrosso, A., Lucibello, C., Saglietti, L., and Zecchina, R. Unreasonable effectiveness of learning neural networks: From accessible states and robust ensembles to basic algorithmic schemes. *Proceedings of the National Academy of Sciences*, 113(48):E7655–E7662, 2016.

Chaudhari, P., Choromanska, A., Soatto, S., LeCun, Y., Baldassi, C., Borgs, C., Chayes, J., Sagun, L., and Zecchina, R. Entropy-SGD: Biassing gradient descent into wide valleys. In *Proceedings of the 5th International Conference on Learning Representations*, 2017.

Claes, Y., Huynh-Thu, V. A., and Geurts, P. Hybrid additive modeling with partial dependence for supervised regression and dynamical systems forecasting. *Machine Learning*, 114(3):72, 2025.

Cohrs, K.-H., Varando, G., Carvalhais, N., Reichstein, M., and Camps-Valls, G. Causal hybrid modeling with double machine learning—applications in carbon flux modeling. *Machine Learning: Science and Technology*, 5(3):035021, 2024.

Dinh, L., Pascanu, R., Bengio, S., and Bengio, Y. Sharp minima can generalize for deep nets. In *Proceedings of the 34th International Conference on Machine Learning*, pp. 1019–1028, 2017.

Dziugaite, G. K. and Roy, D. M. Computing nonvacuous generalization bounds for deep (stochastic) neural networks with many more parameters than training data. In *Proceedings of the 33rd Conference on Uncertainty in Artificial Intelligence*, 2017.

Foret, P., Kleiner, A., Mobahi, H., and Neyshabur, B. Sharpness-aware minimization for efficiently improving generalization. In *Proceedings of the 9th International Conference on Learning Representations*, 2021.

Forsslund, U. and Lindskog, P. Combining semi-physical and neural network modeling: An example of its usefulness. *IFAC Proceedings Volumes*, 30(11):767–770, 1997.

Gamella, J. L., Peters, J., and Bühlmann, P. Causal chambers as a real-world physical testbed for AI methodology. *Nature Machine Intelligence*, 7:107–118, 2025.

Gao, J., Michelis, M. Y., Spielberg, A., and Katzschmann, R. K. Sim-to-real of soft robots with learned residual physics. *IEEE Robotics and Automation Letters*, 9(10):8523–8530, 2024.

Giampiccolo, S., Reali, F., Fochesato, A., Iacca, G., and Marchetti, L. Robust parameter estimation and identifiability analysis with hybrid neural ordinary differential equations in computational biology. *npj Systems Biology and Applications*, 10(1):139, 2024.

Guillaume, J. H., Jakeman, J. D., Marsili-Libelli, S., Asher, M., Brunner, P., Croke, B., Hill, M. C., Jakeman, A. J., Keesman, K. J., Razavi, S., and Stigter, J. D. Introductory overview of identifiability analysis: A guide to evaluating whether you have the right type of data for your modeling purpose. *Environmental Modelling & Software*, 119:418–432, 2019.

Haußmann, M., Gerwinn, S., Look, A., Rakitsch, B., and Kandemir, M. Learning partially known stochastic dynamics with empirical PAC Bayes. In *Proceedings of the 24th International Conference on Artificial Intelligence and Statistics*, pp. 478–486, 2021.

Heiden, E., Millard, D., Coumans, E., Sheng, Y., and Sukhatme, G. S. NeuralSim: Augmenting differentiable simulators with neural networks. In *Proceedings of 2021 IEEE International Conference on Robotics and Automation*, pp. 9474–9481, 2021.

Hinton, G. E. and van Camp, D. Keeping the neural networks simple by minimizing the description length of the weights. In *Proceedings of the 6th Annual Conference on Computational Learning Theory*, pp. 5–13, 1993.

Hochreiter, S. and Schmidhuber, J. Flat minima. *Neural Computation*, 9(1):1–42, 1997.

Holt, S., Liu, T., and van der Schaar, M. Automatically learning hybrid digital twins of dynamical systems. In *Advances in Neural Information Processing Systems 37*, pp. 72170–72218, 2024.

Izmailov, P., Podoprikhin, D., Garipov, T., Vetrov, D., and Wilson, A. G. Averaging weights leads to wider optima and better generalization. In *Proceedings of the 34th Conference on Uncertainty in Artificial Intelligence*, 2018.

Kashtanova, V., Ayed, I., Arrieula, A., Potse, M., Gallinari, P., and Sermesant, M. Deep learning for model correction in cardiac electrophysiological imaging. In *Proceedings of the 5th International Conference on Medical Imaging with Deep Learning*, pp. 665–675, 2022.

Keskar, N. S., Mudigere, D., Nocedal, J., Smelyanskiy, M., and Tang, P. T. P. On large-batch training for deep learning: Generalization gap and sharp minima. In *Proceedings of the 5th International Conference on Learning Representations*, 2017.

Kim, M., Li, D., Hu, S. X., and Hospedales, T. Fisher SAM: Information geometry and sharpness aware minimisation. In *Proceedings of the 39th International Conference on Machine Learning*, pp. 11148–11161, 2022.

Kwon, J., Kim, J., Park, H., and Choi, J. K. ASAM: Adaptive sharpness-aware minimization for scale-invariant learning of deep neural networks. In *Proceedings of the 38th International Conference on Machine Learning*, pp. 5905–5914, 2021.

Mehta, V., Char, I., Neiswanger, W., Chung, Y., Nelson, A. O., Boyer, M. D., Kolemen, E., and Schneider, J. Neural dynamical systems: Balancing structure and flexibility in physical prediction. In *Proceedings of the 2021 IEEE Conference on Decision and Control*, pp. 3735–3742, 2021.

Miller, A. C., Foti, N. J., and Fox, E. Learning insulin-glucose dynamics in the wild. In *Proceedings of the 5th Machine Learning for Healthcare Conference*, pp. 172–197, 2020.

Palumbo, E., Saengkyongam, S., Cervera, M. R., Behrmann, J., Miller, A. C., Sapiro, G., Heinze-Deml, C., and Wehenkel, A. Hybrid modeling of photoplethysmography for non-invasive monitoring of cardiovascular parameters, 2025.

Psichogios, D. C. and Ungar, L. H. A hybrid neural network-first principles approach to process modeling. *AIChE Journal*, 38(10):1499–1511, 1992.

Qian, Z., Zame, W. R., Fleuren, L. M., Elbers, P., and van der Schaar, M. Integrating expert ODEs into neural ODEs: Pharmacology and disease progression. In *Advances in Neural Information Processing Systems 34*, pp. 11364–11383, 2021.

Rico-Martínez, R., Anderson, J. S., and Kevrekidis, I. G. Continuous-time nonlinear signal processing: A neural network based approach for gray box identification. In *Proceedings of the IEEE Workshop on Neural Networks for Signal Processing*, pp. 596–605, 1994.

Rissanen, J. Modeling by shortest data description. *Automatica*, 14(5):465–471, 1978.

Rudolph, M., Kurz, S., and Rakitsch, B. Hybrid modeling design patterns. *Journal of Mathematics in Industry*, 14(1):3, 2024.

Salzmann, T., Kaufmann, E., Arrizabalaga, J., Pavone, M., Scaramuzza, D., and Ryll, M. Real-time neural MPC: Deep learning model predictive control for quadrotors and agile robotic platforms. *IEEE Robotics and Automation Letters*, 8(4):2397–2404, 2023.

Schweidtmann, A. M., Zhang, D., and Von Stosch, M. A review and perspective on hybrid modeling methodologies. *Digital Chemical Engineering*, 10:100136, 2024.

Senouf, O., Wehenkel, A., Vincent-Cuaz, C., Abbé, E., and Frossard, P. Inductive domain transfer in misspecified simulation-based inference. In *Neural Information Processing Systems 38*, 2025.

Shirakami, R., Kitahara, T., Takeuchi, K., and Kashima, H. QTNet: Theory-based queue length prediction for urban traffic. In *Proceedings of the 29th ACM SIGKDD Conference on Knowledge Discovery and Data Mining*, pp. 4832–4841, 2023.

Takeishi, N. and Kalousis, A. Physics-integrated variational autoencoders for robust and interpretable generative modeling. In *Advances in Neural Information Processing Systems 34*, pp. 14809–14821, 2021.

Takeishi, N. and Kalousis, A. Deep grey-box modeling with adaptive data-driven models toward trustworthy estimation of theory-driven models. In *Proceedings of the 26th International Conference on Artificial Intelligence and Statistics*, pp. 4089–4100, 2023.

Thompson, M. L. and Kramer, M. A. Modeling chemical processes using prior knowledge and neural networks. *AIChE Journal*, 40(8):1328–1340, 1994.

Thoreau, R., Risser, L., Achard, V., Berthelot, B., and Briottet, X. Physics-informed variational autoencoders for improved robustness to environmental factors of variation. *Machine Learning*, 114:198, 2025.

Tsuzuku, Y., Sato, I., and Sugiyama, M. Normalized flat minima: Exploring scale invariant definition of flat minima for neural networks using PAC-bayesian analysis. In *Proceedings of the 37th International Conference on Machine Learning*, pp. 9636–9647, 2020.

Tushar and Chakraborty, S. Deep physics corrector: A physics enhanced deep learning architecture for solving stochastic differential equations. *Journal of Computational Physics*, 479:112004, 2023.

Verma, Y., Heinonen, M., and Garg, V. ClimODE: Climate and weather forecasting with physics-informed neural ODEs. In *Proceedings of the 12th International Conference on Learning Representations*, 2024.

Wehenkel, A., Behrmann, J., Hsu, H., Sapiro, G., Louppe, G., and Jacobsen, J.-H. Robust hybrid learning with expert augmentation. *Transactions of Machine Learning Research*, 2023.

Wehenkel, A., Gamella, J. L., Sener, O., Behrmann, J., Sapiro, G., Cuturi, M., and Jacobsen, J.-H. Addressing misspecification in simulation-based inference through data-driven calibration. In *Proceedings of the 42nd International Conference on Machine Learning*, pp. to appear, 2025.

Wieland, F.-G., Hauber, A. L., Rosenblatt, M., Tönsing, C., and Timmer, J. On structural and practical identifiability. *Current Opinion in Systems Biology*, 25:60–69, 2021.

Xu, W., Ling, F., Han, T., Chen, H., Ouyang, W., and Bai, L. Generalizing weather forecast to fine-grained temporal scales via physics-AI hybrid modeling. In *Advances in Neural Information Processing Systems*, volume 37, pp. 23325–23351, 2024.

Ye, Y., Tolou, M., Vadhavkar, S., Jiang, X., Liu, H., and Wang, L. On the identifiability of hybrid deep generative models: Meta-learning as a solution. In *Advances in Neural Information Processing Systems 37*, pp. 7714–7735, 2024.

Yin, Y., Le Guen, V., Dona, J., de Bézenac, E., Ayed, I., Thome, N., and Gallinari, P. Augmenting physical models with deep networks for complex dynamics forecasting. In *Proceedings of the 9th International Conference on Learning Representations*, 2021.

Zhuang, J., Gong, B., Yuan, L., Cui, Y., Adam, H., Dvornek, N., Tatikonda, S., Duncan, J., and Liu, T. Surrogate gap minimization improves sharpness-aware training. In *Proceedings of the 10th International Conference on Learning Representations*, 2022.

Zou, B. J., Levine, M. E., Zaharieva, D. P., Johari, R., and Fox, E. Hybrid<sup>2</sup> neural ODE causal modeling and an application to glycemic response. In *Proceedings of the 41st International Conference on Machine Learning*, pp. 62934–62963, 2024.

## A. Task Description

### A.1. Pendulum Time-Series

#### A.1.1. DATA

We simulated the damped pendulum system:

$$\ddot{v}(t) + \gamma \dot{v}(t) + (2\pi\omega)^2 \sin v(t) = 0,$$

where  $v(t) : \mathbb{R} \rightarrow \mathbb{R}$  is the pendulum's angle, and  $\ddot{v}$  and  $\dot{v}$  denote the second and first derivatives with regard to time  $t \in \mathbb{R}$ , respectively. For the simulation we used the explicit Runge-Kutta method of order 5(4) for the numerical integration with a time step of 0.02. We then subsampled the sequence by a factor of 10, so the effective time step of the data is  $\Delta t = 0.2$ . We set  $\gamma = 0.5$  and  $\omega = 2/3$  for data generation.

We formulate the task as the prediction from an initial state  $x$  to a subsequent sequence of states  $y$ :

$$\begin{aligned} x &= \mathbf{v}(0) \in \mathbb{R}^2 \quad \text{and} \\ y &= [\mathbf{v}(\Delta t), \dots, \mathbf{v}(m_y \Delta t)] \in \mathbb{R}^{m_y \times 2}, \end{aligned}$$

where  $\mathbf{v} = [v, \dot{v}]$ , and  $m_y = 10$  is the output sequence lengths. The initial angle  $v(0)$  and angular velocity  $\dot{v}(0)$  were randomly sampled from the uniform distribution  $U(-\pi/2, \pi/2)$ . We generated 25, 25, and 25 input-output pairs for the training, validation, and test data, respectively. We added zero-mean Gaussian noise with standard deviation 0.01 to the data. Similar data were also used in [Yin et al. \(2021\)](#).

#### A.1.2. MODEL

The hybrid model we used is a hybrid neural ODE as practiced in [Yin et al. \(2021\)](#). We suppose that we know a part of the data-generating equation as an incomplete scientific model:

$$f_\theta(v) := \ddot{v}(t) + (2\pi\tilde{\omega})^2 \sin v(t),$$

where  $\theta = \{\tilde{\omega}\}$  is the unknown parameter to be identified. Then the hybrid neural ODE is formulated as

$$y = \text{ODESolve}(f_\theta(v) + g_\phi(v) = 0; v(0) = x)$$

where  $g_\phi$  is a feed-forward neural net with two hidden layers of size 128 and the ReLU activation function.

### A.2. Reaction-Diffusion

#### A.2.1. DATA

We simulated the FitzHugh-Nagumo type reaction-diffusion system:

$$\begin{aligned} u_t(t, \xi) &= a \nabla^2 u + u - u^3 - \kappa - v, \\ v_t(t, \xi) &= b \nabla^2 v + u - v, \end{aligned}$$

where  $u(t, \xi), v(t, \xi) : \mathbb{R} \times [-1, 1]^2 \rightarrow \mathbb{R}$  are the concentrations of two chemical species at time  $t \in \mathbb{R}$  and spatial location  $\xi \in [-1, 1]^2$ .  $u_t$  and  $v_t$  denote the temporal derivatives of  $u$  and  $v$ , respectively.  $\nabla^2$  is the Laplacian operator with regard to the space. For the simulation we used the explicit Runge-Kutta method of order 5(4) for the numerical integration with a time step of 0.001. We then subsampled the sequence by a factor of 100, so the effective time step of the data is  $\Delta t = 0.1$ . We set  $a = 0.001$ ,  $b = 0.005$ , and  $\kappa = 0.005$  for data generation.

The task is to predict from an initial state  $x \in \mathbb{R}^{2 \times d \times d}$  to the subsequent sequence of states  $y \in \mathbb{R}^{2 \times d \times d \times m_y}$ , where  $d = 32$  is the number of spatial discretization points along each axis, and  $m_y = 5$  is the output sequence length. We used the five-point stencil method for approximating the Laplacian operator. The initial concentrations  $u(0, \xi)$  and  $v(0, \xi)$  were generated by sampling from the uniform distribution  $U(0, 1)$ . We generated 100, 100, and 100 input-output pairs for the training, validation, and test data, respectively. We added zero-mean Gaussian noise with standard deviation 0.01 to the data. Similar data were also used in [Yin et al. \(2021\)](#).

### A.2.2. MODEL

We set an incomplete scientific model as the diffusion terms:

$$f_\theta(u, v) := \begin{bmatrix} u_t - \tilde{a} \nabla^2 u \\ v_t - \tilde{b} \nabla^2 v \end{bmatrix},$$

where  $\theta = \{\tilde{a}, \tilde{b}\}$  is the unknown parameters to be identified. It is combined with a machine learning part  $g_\phi$  implemented as a convolutional neural net (kernel size 3) with two hidden layers of size (i.e., number of channels) 16, the ReLU activation function, and batch normalization. The combination is formulated as

$$y = \text{ODESolve}(f_\theta(u, v) + g_\phi(u, v) = 0; v(0) = x).$$

## A.3. Duffing Oscillator

### A.3.1. DATA

We simulated a nonlinear oscillator system:

$$\ddot{v}(t) + \alpha v(t) - \beta v(t)^3 = 0.$$

For the simulation we used the explicit Runge-Kutta method of order 5(4) for the numerical integration with a time step of 0.005. We then subsampled the sequence by a factor of 20, so the effective time step of the data is  $\Delta t = 0.1$ . We set  $\alpha = 1$  and  $\beta = 1$  for data generation.

We formulate the task as the prediction from an initial condition  $x$  to a subsequent states  $y$  of length  $m_y$ :

$$\begin{aligned} x &= \mathbf{v}(0) \in \mathbb{R}^2 \quad \text{and} \\ y &= [\mathbf{v}(\Delta t), \dots, \mathbf{v}(m_y \Delta t)] \in \mathbb{R}^{m_y \times 2}, \end{aligned}$$

where  $\mathbf{v} = [v, \dot{v}]$ , and  $m_y = 10$  is the output sequence lengths. We generated 100, 100, and 100 input-output pairs for the training, validation, and test data, respectively. We added zero-mean Gaussian noise with standard deviation 0.01 to the data.

### A.3.2. MODEL

We set an incomplete scientific model:

$$f_\theta(v) := \ddot{v}(t) + \tilde{\alpha} v(t),$$

where  $\theta = \{\tilde{\alpha}\}$  is the unknown parameter to be identified. The hybrid model is a hybrid neural ODE:

$$y = \text{ODESolve}(f_\theta(v) + g_\phi(v) = 0; v(0) = x)$$

where  $g_\phi$  is a feed-forward neural net with two hidden layers of size 128 and the ReLU activation function.

## A.4. Pendulum Images

### A.4.1. DATA

We simulated trajectories of a pendulum as in the PENDULUM TIME-SERIES task and then rendered gray-scale images of size  $d \times d$  with  $d = 48$  pixels based on the simulated pendulum angles. The task is to predict future image sequences,  $y \in [0, 1]^{m_y \times d \times d}$ , given a preceding sequence of images,  $x \in [0, 1]^{m_x \times d \times d}$ , where  $m_x = 10$  and  $m_y = 10$  are the input and output sequence length, respectively. We generated 200, 200, and 200 input-output pairs for the training, validation, and test data, respectively.

### A.4.2. MODEL

The hybrid model is built by combining the hybrid neural ODE used in the PENDULUM TIME-SERIES task and additional neural nets for encoding and decoding. The model has two encoders. The first encoder receives the input image sequence and gives the initial condition of the pendulum for the hybrid neural ODE. The second encoder receives the input image

sequence and gives a latent representation, which is then concatenated with the output of the hybrid neural ODE. The decoder maps the output of the hybrid neural ODE (pendulum angles), concatenated with the latent representation, to images. It comprises 1) a network with fully-connected layers with two hidden layers of size 1152 with ReLU and 2) a convolutional network (kernel size 3) with two hidden layers of size (i.e., number of channels) 576 and 288 with ReLU and batch normalization.

Note that the absolute initial condition of the pendulum is in principle unidentifiable because we do not give any correspondence between the images and the pendulum angles. However it is not problematic here because we focus on the estimation of the pendulum’s frequency parameter,  $\theta = \{\tilde{\omega}\}$ , and the interest is not on the phase of the oscillation. The encoder should learn the map from images to the initial condition only up to the translational invariance.

## A.5. Wind Tunnel

### A.5.1. DATA

We used a part of the dataset by [Gamella et al. \(2025\)](#)<sup>1</sup>. It is a dataset comprising measurements from a real-world wind tunnel. We extracted a subset of the data (“loads\_hatch\_mix\_fast\_run” of “wt\_walks\_v1” dataset) to formulate a task to predict a sequence of the pressure inside the tunnel  $y \in \mathbb{R}^m$  from a sequence of the loads of the intake and exhaust fans and the position of the hatch,  $x \in \mathbb{R}^{m \times 3}$ , where  $m$  is the length of the input and output sequences. The hatch controls an additional opening at the middle of the tunnel. We created the subsequences  $\{(x, y)\}$  by a sliding window of length  $m = 200$  with a stride of 50 from the original time series. Finally we have 600, 150, and 235 input-output pairs for the training, validation, and test data, respectively.

### A.5.2. MODEL

As an incomplete scientific model  $f_\theta$ , we use the models “A1” and “C2” presented in [Gamella et al. \(2025\)](#), which give the relation between the pressure and the fan loads. They are incomplete in terms of the effect of the hatch position and the transient dynamics of the pressure. The hybrid model transforms the output of these models with a feed-forward neural net. We set a scalar parameter of the model C2, namely the ratio  $r \in [0, 1]$  of the maximum airflow that the fans produce at full speed, as the unknown parameter to be estimated, i.e.,  $\theta = \{r\}$ . As the truly data-generating value of the parameter is never known, we used a value suggested in the paper and the codes ([Gamella et al., 2025](#)),  $r = 0.7$ , as a reference value to compute the estimation error of  $\theta$ . The full hybrid model is

$$y = g_\phi(z, x),$$

where  $z = f_\theta(x) \in \mathbb{R}^m$  is the output of the scientific model, and  $g_\phi$  is a feed-forward neural net with two hidden layers of size  $2m$  and the ReLU activation function.

## A.6. Light Tunnel

### A.6.1. DATA

We used another part of the dataset by [Gamella et al. \(2025\)](#)<sup>1</sup>. It contains real-world measurements from a light tunnel made of light sources, linear polarizers, and a light sensor. We extracted a subset of the data (“uniform\_ap\_1.8\_iso\_500.0\_ss\_0.005” of “lt\_camera\_v1” dataset) to formulate a task to predict the RGB image taken by the sensor,  $y \in [0, 1]^{3 \times 100 \times 100}$ , from the light source configuration and the polarizer angles,  $x = [R \ G \ B \ \alpha_1 \ \alpha_2] \in \mathbb{R}^5$ .  $R, G, B$  are the intensities of the red, green, and blue light sources, respectively, and  $\alpha_1, \alpha_2$  are the angles of the two polarizers. Finally we have 6000, 1000, and 2500 input-output pairs for the training, validation, and test data, respectively.

### A.6.2. MODEL

As an incomplete scientific model,  $f_\theta$ , we use the model “F3” presented in [Gamella et al. \(2025\)](#), which models the effect of the polarizers in a frequency-dependent way:

$$\begin{bmatrix} \tilde{R} \\ \tilde{G} \\ \tilde{B} \end{bmatrix} = \min \left( 1, e \operatorname{diag}(\mathbf{w}) \mathbf{S} \operatorname{diag}((\mathbf{t}^p - \mathbf{t}^c) \cos^2(\alpha_1 - \alpha_2) + \mathbf{T}^c) \begin{bmatrix} R \\ G \\ B \end{bmatrix} \right) \quad (7)$$

<sup>1</sup><https://github.com/juangamella/causal-chamber>

We used the value of  $e$  and  $S$  suggested in the paper and the codes (Gamella et al., 2025). The remaining,  $\mathbf{w} \in \mathbb{R}^3$ ,  $\mathbf{t}^p \in \mathbb{R}^3$ , and  $\mathbf{t}^c \in \mathbb{R}^3$ , are treated as unknown parameters to be estimated, i.e.,  $\theta \in \mathbb{R}^9$ . As evident from Equation (7), the magnitude of these parameters are inherently unidentifiable. We thus compared the estimation results and the reference values suggested in the paper and the codes (Gamella et al., 2025) with the cosine similarity. Given  $\tilde{R}$ ,  $\tilde{G}$ , and  $\tilde{B}$  computed by Equation (7), then  $f_\theta$  outputs an image by replicating the RGB values spatially in a hexagonal shape resembling the light placement pattern. The full hybrid model further transforms such an image with a convolutional neural net with U-Net architecture.

## B. Learning and Model Selection

For all tasks and learning strategies, we used the Adam optimizer for setting adaptive learning rates. The overall learning rate of Adam was set to  $10^{-4}$  for PENDULUM TIME-SERIES, REACTION-DIFFUSION, and DUFFING OSCILLATOR;  $3 \times 10^{-4}$  for WIND TUNNEL; and  $10^{-3}$  for PENDULUM IMAGES and LIGHT TUNNEL. We run the optimization for 20000 iterations. We did full-batch training for PENDULUM TIME-SERIES, REACTION-DIFFUSION, DUFFING OSCILLATOR, and WIND TUNNEL; and mini-batch training with a batch size of 50 for PENDULUM IMAGES and LIGHT TUNNEL. We applied the cosine annealing schedule for the learning rate with a single period over the entire training iterations, i.e., the learning rate is gradually decreased from the initial value to  $10^{-6}$ .

We report the performance of a model that achieved the best  $\theta$ -error for all the methods. Although it is against the normal practice to select models by validation prediction errors, we had to do so because the  $y$ -error and  $\theta$ -error are usually not consistent with finite training and validation datasets; it is, in the first place, the cause of our headache in hybrid modeling! If the validation/test prediction error was a good proxy of the parameter estimation error, we (and other researchers) would not have done such a lot of research on this topic. To maintain the comparison fair, we applied this model selection strategy not only to the proposed methods but also to all the baseline methods.

## C. More Results

### C.1. Sensitivity to Hyperparameters

In Figure 5, we report the full result of the sensitivity of parameters with regard to the hyperparameter configurations.

### C.2. Learning with Varying Scientific Parameters

We addressed a more challenging problem setting, where the data are generated by varying values of  $\theta$ .

For the PENDULUM TIME-SERIES task, we randomly sampled  $\omega$  from the uniform distribution  $U(0.1, 1.0)$  for each input-output pair. The input  $x$  is now a sequence  $x = [\mathbf{v}(-(m_x - 1)\Delta t), \dots, \mathbf{v}(0)] \in \mathbb{R}^{m_x \times 2}$ , where  $m_x = 10$  is the input sequence length, instead of the mere initial condition  $\mathbf{v}(0)$  in the original task. We added an encoder network to the model, which receives the input sequence and outputs an estimate of  $\omega$ . The encoder network is a feed-forward neural net with two hidden layers of size 256 and the ReLU activation function.  $x$  is first flattened to a vector before feeding it to the encoder.

We altered the REACTION-DIFFUSION task similarly to the above. We randomly sampled  $a$  and  $b$  from the uniform distributions  $U(0, 0.02)$  and  $U(0, 0.02)$ , respectively, for each input-output pair. The input  $x$  is now a sequence of 2-channel 2-D fields of size  $2 \times d \times d \times m_x$  with length  $m_x = 5$ . The encoder network comprises a convolutional network and a feed-forward network with fully-connected layers. The convolutional net is with two hidden layers of size 288 and 144, the ReLU activation function, and batch normalization. We feed the input  $x$  to the convolutional net by first flattening the temporal dimension into the channel dimension. Its output is then fed to the feed-forward net, which has one hidden layer of size 256 and the ReLU activation function.

For the DUFFING OSCILLATOR task, we randomly sampled  $\alpha$  from the uniform distribution  $U(0, 2)$  for each input-output pair. The input  $x$  is now a sequence of length  $m_x = 10$ . The encoder network is a feed-forward neural net with two hidden layers of size 256 and the ReLU activation function.

In Figure 6, we show the outputs of the encoder networks. Most notably, in the DUFFING OSCILLATOR task, the encoder learned with `fsam` infers  $\theta$  with better correlation to the data-generating values, compared to the `erm` case. Meanwhile there remain nonnegligible variances in the inferred values, which suggests the difficulty of the problem. On the other hand, the results of the REACTION-DIFFUSION task show almost no difference between the two methods, which implies that the task is relatively easy.

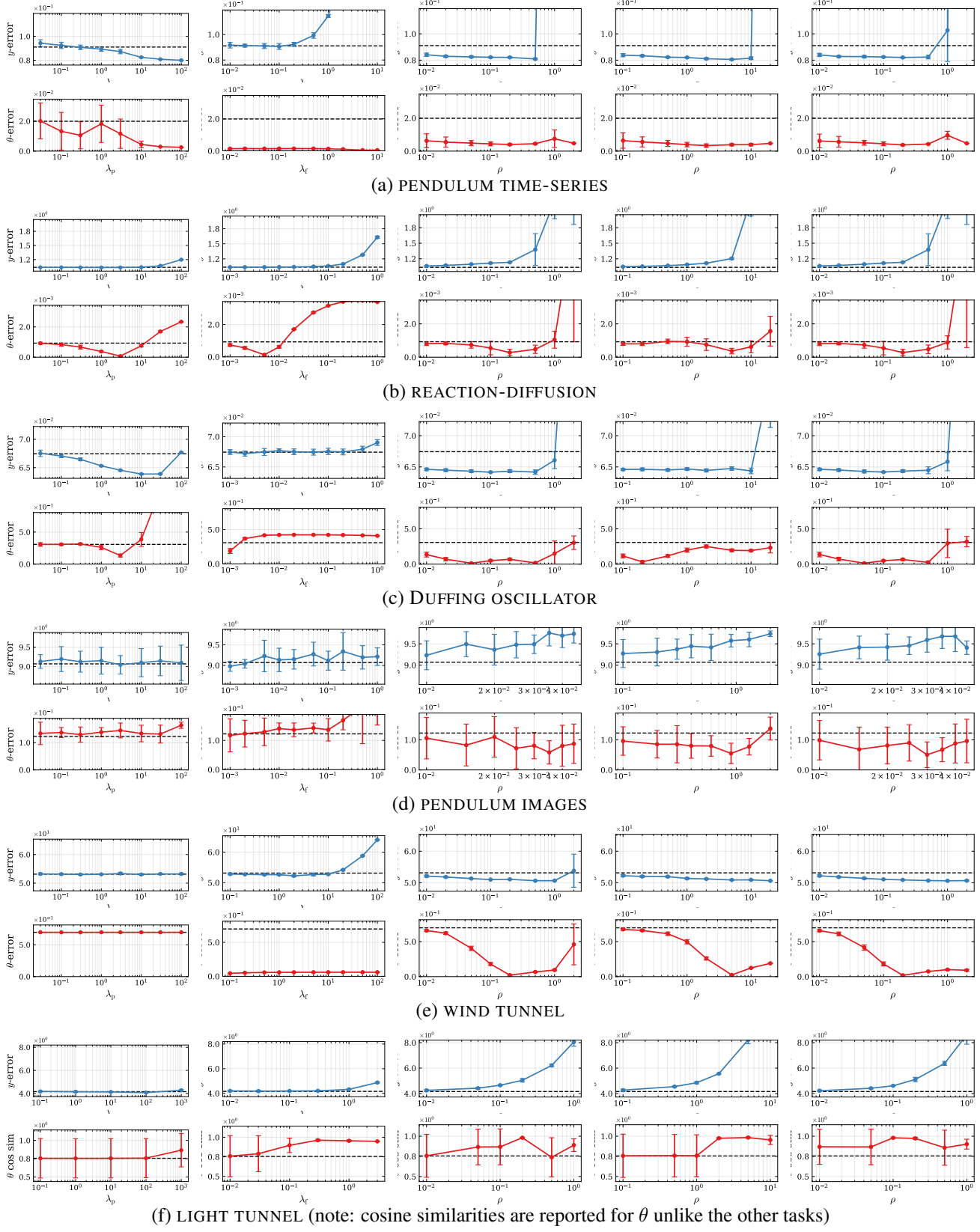


Figure 5. Sensitivity of performance with regard to the hyperparameter configurations.

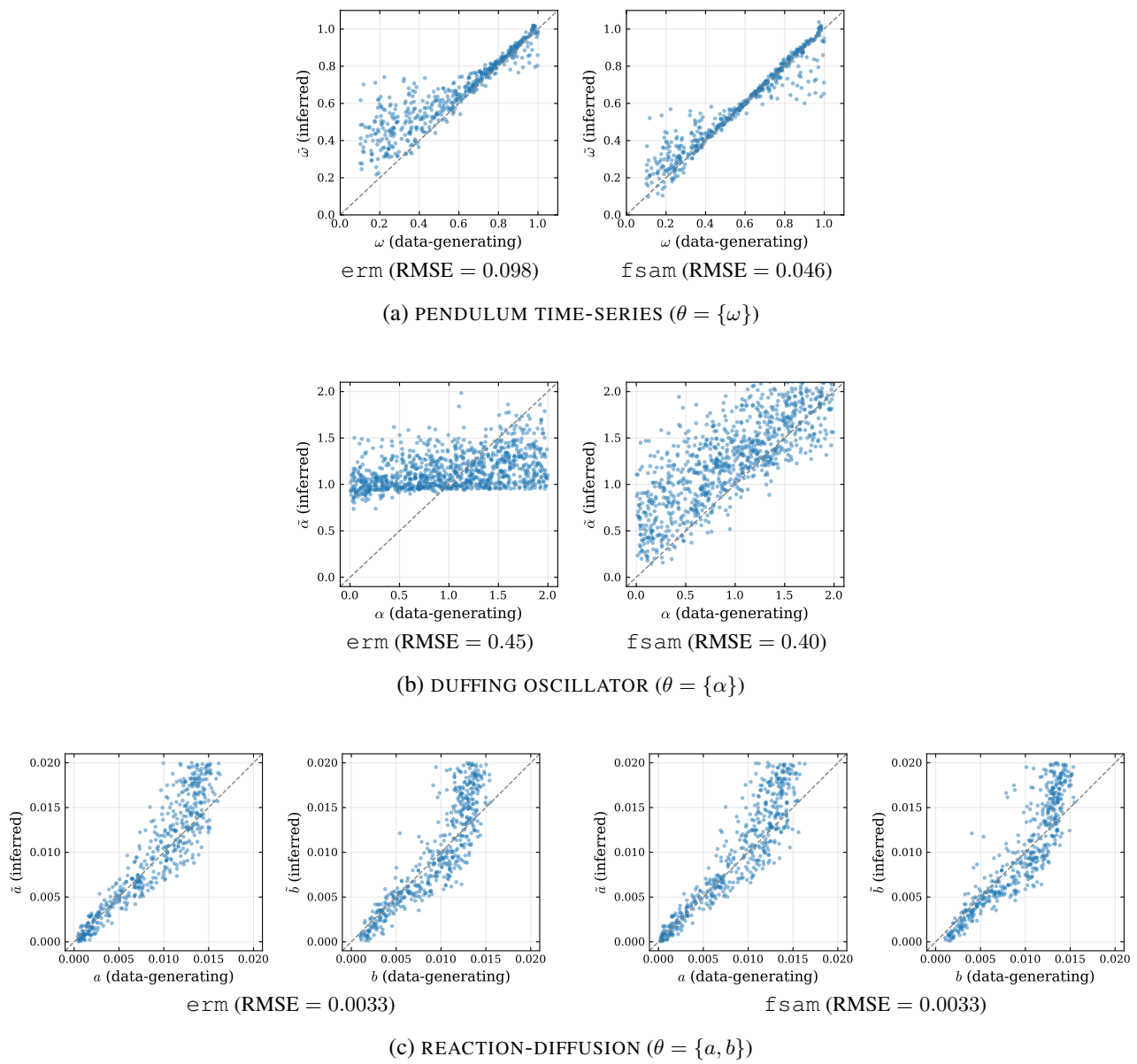


Figure 6. Inferred values of the parameters of the scientific model part,  $\theta$ .